Generalized locomotion of brittle stars with an arbitrary number of arms

Daiki Wakita[1], Katsushi Kagaya[2,3], Hitoshi Aonuma[1,4]*

[1]Graduate School of Life Science; Hokkaido University; Sapporo, Hokkaido, 060-0810; Japan

[2]The Hakubi Center for Advanced Research; Kyoto University; Yoshida-Konoe, Kyoto, 606-8501; Japan

[3]Seto Marine Biological Laboratory, Field Science, Education and Research Center; Kyoto University; Shirahama, Wakayama, 649-2211; Japan

[4]Research Institute for Electronic Science; Hokkaido University; Sapporo, Hokkaido, 060-0812; Japan

*Correspondence to Hitoshi Aonuma, who serves as the Lead Contact for this paper. Research Center of Mathematics for Social Creativity, Research Institute for Electronic Science, Hokkaido University, Sapporo 060-0812, Japan.

Tel/Fax: +81-11-706-3832, Email: aon@es.hokudai.ac.jp

Abstract

Typical brittle stars creep on the ground with five arms. However, some species of them show individual difference in the number of arms: commonly five or six, rarely four or seven. We found this trait unique since intact legged animals each own a fixed number of limbs in general. How does a single species manage different numbers of motile organs to realize adaptive locomotion? We aim to describe four- to seven-armed locomotion to explore a common rule across different arm numbers in brittle stars. Gathering several quantitative indices obtained from *Ophiactis brachyaspis*, we figured out an average locomotion where a front position emerges at one of the second neighboring arms to a mechanically stimulated arm, while side arms adjacent to the front synchronously work as left and right rowers, regardless of the number of arms. This idea would generalize how ‘left and right’ emerges in a radially symmetrical body.

Introduction

Legged animals utilize appendages to move around on the ground. In most cases, intact adults of each species have a constant number of motile organs, such as four in many mammals and six in most insects. Supposedly, each species adopts a number-specific mechanism of locomotion. In this context, some species of brittle stars (Echinodermata: Ophiuroidea) exhibit an appealing individual difference, where some intact individuals have five appendages or less, while others have six or more (Figure S1). This difference in number is usually found in fissiparous species, which undergo asexual reproduction by fission and regeneration [1–3].

As typical echinoderms show pentaradial symmetry, most ophiuroid species standardly have five multi-jointed appendages called "arms," which extend from the "disk" at the center. Previous studies have described arm movements in the locomotion of five-armed species in qualitative terms [4–10] as well as in quantitative terms [11, 12]. Several locomotor modes have been known even in a single species. An often reported mode, referred to as "breast stroke" [8, 9] or "rowing" [11], is characterized by a leading arm facing forward, two side arms working as left and right rowers, and two back arms dragged passively [4, 5, 7–9, 11, 12]. Some studies have observed another locomotor mode, called as "paddling" [8] or "reverse rowing" [11], where a backmost arm is dragged while the other four actively row [5–8, 11]. The ophiuroid body creeps in a certain direction with such bilaterally coordinated manners [11]. Since the 'role' of each arm switches when the body changes moving direction [11], brittle stars do not have consistent antero-posterior and left-right axes in behavior.

Although the five-armed locomotion in common brittle stars and the individual difference in specific species have been viewed in different contexts, none has combined them to spotlight ophiuroid locomotion under the different numbers of arms. Referring to the human body, whether the body comprises five, six, or other numbers of modules seems to bring a huge issue in individual function. How do these animals manage the difference in the number of motile organs to realize adaptive locomotion within a species? The aim of our study is to quantitatively describe the four-, five- six-, and seven-armed locomotion in the intact individual of an ophiuroid species, *Ophiactis brachyaspis* Clark, 1911 (Figure S1), to explore a common rule across different arm numbers. Figuring out a control law which is flexible with the number of limbs, we would understand what sorts of body structure and interaction are of great or little importance to adaptive movements, and further apply such capacity in nature to a more flexible design in robotics. We will also provide a general scheme of how 'left and right'—'front and back' in the same time—emerges in a multidirectional body with an arbitrary number of rays to make a unidirectional behavior. Since this study addresses a generalized description in many-sided aspects, we take the approach of "exploratory data analysis" [13, 14] with Bayesian statistical modeling, less weighting confirmation of a fixed hypothesis. One conclusion through our study is that a mechanical stimulus to an arm averagely makes one of its *second* neighboring arms be a leading arm, with the leader's side arms working as left and right synchronous rowers. Thus regardless of the total number of arms, ophiuroid locomotion shows a common anterior pattern, which could be positioned by counting how many arms some signal passes along a circular pathway.

Results

Moving direction (Θ)

The measured data of the post-stimulus moving direction Θ (Figures S2, S3; Equation 1 in Materials and Methods) are shown in Figure 1 by dot plots. For all the four-, five-, six-, and seven-armed cases, the model assuming a mixture of two von Mises distributions in Θ yielded smaller WAICs—better predictabilities—than that assuming a single distribution (Table 1). Compared with the small Δ (difference from the best one; Equation 12 in Materials and Methods) of the one-distribution model in four- and five-armed animals, the six- and seven-armed Δ values were larger enough to interpret that bimodality was more obvious in more arms. Following the better model in terms of WAIC, we hereafter show the results on the assumption of two distributions for all the cases.

The posterior medians of two distributions' means, which were calculated separately for the negative and positive ranges, were ±17, ±29, ±46, and ±70 in four- to seven-armed animals, respectively. These estimated values signify that the more arms a brittle star had, the further two distributions of Θ were apart from each other (Figure 1). In other words, the average moving direction of individuals with more arms was more angled from the opposite direction of the stimulated arm. Predictive distribution of Θ indeed depicted this trend (Figure 1).

Left or right rower (B_α)

The measured data of B_α—the α-th arm's degree of being a left or right rower (Figures S2, S3; Equation 3 in Materials and Methods)—are schematized trial-by-trial in Figures S1–S4. As for the five- and six-armed populations, no-individuality models consistently took smaller WAICs than their counterparts where individuality was assigned to the mean of B_α (Table 1). We thus avoid mentioning individual difference within the same arm number.

Among L_α, S, Θ, Θ_{sign}, and F_α, the five-armed B_α was better explained by the continuous moving direction Θ, whereas the six- and seven-armed cases rather emphasized its sign Θ_{sign} (Equation 2 in Materials and Methods) in discrete terms (Table 1). In four arms, the arm length L_α was chosen for a best explanatory variable although Θ showed a close performance. Given the dominance of the moving direction indicators as well as Θ's bimodality (Figure 1), we present the data of B_α separately by Θ_{sign}—in which side moving direction angled from the midline of the stimulated arm. Two groups were here defined by whether it angled clockwise ($\Theta_{\text{sign}} = 0$) or anticlockwise ($\Theta_{\text{sign}} = 1$).

The Θ_{sign}-based grouping exhibited a common locomotor mode among four-, five-, six-, and seven-armed animals in regards to B_α's posterior means. The directional property of each arm could be explained by how many arms we count from the stimulated arm. Primarily, one of the *first* neighboring arms to the stimulated arm consistently took the largest or second largest $|B_\alpha|$—absolute values of posterior means (Figures 2–5A,C). This *first* arm corresponds to the anticlockwise neighbor of the arm 1 when $\Theta_{\text{sign}} = 0$ (Figures 2–5A) and the clockwise one when $\Theta_{\text{sign}} = 1$ (Figures 2–5C). In the next place, the *second* neighbor from the stimulus—next to the *first* in the same detour—took the smallest or second smallest $|B_\alpha|$. Then, the *third* neighbor of the stimulus—next to the *second*—took the largest or second largest $|B_\alpha|$ which was opposite in sign to that of the *first*. One exception was the seven-armed case when $\Theta_{\text{sign}} = 0$ (Figure 5A); the *second* (arm 3) and the *third* (arm 4) respectively had the fourth smallest and the third largest, probably due to the outlying trial shown at the row 1 of column 4 in Figure S7. Replacing the ordinary cases' values with actual movements, the *first* actively pushed in the direction of the stimulated arm, while the *third* actively pushed oppositely to the *first*. These movements could make the *second* face forward, which indeed corresponded to the ranges of Θ in all the cases (Figures 2–5A,C; see also Videos S1, S2).

Synchronization between two arms ($E_{\alpha\beta}$)

The higher explanatory power of Θ_{sign} could also apply to the instance of the degree of synchronization between the α- and β-th arms, $E_{\alpha\beta}$ (Equation 4 in Materials and Methods), because five-, six-, and seven-armed animals each brought the smallest WAIC in the model assuming Θ_{sign}'s effect (Table 1). In the four-armed case, the model without an explanatory variable best performed while the presence of Θ or Θ_{sign} resulted in similar predictabilities. Accenting the significance of Θ_{sign} as with B_α's situation, we here show the resultant values of $E_{\alpha\beta}$ discretely by the sign of Θ.

A side-by-side comparison with the Θ_{sign}-based results of B_α shows us that the pair of the *first* and *third* rowers counting from the stimulus had the negatively largest medians of $E_{\alpha\beta}$'s posterior means in most cases (Figures 2–5B,D). Although one exception was found in the seven-armed with $\Theta_{\text{sign}} = 0$, the pair's value E_{24} leaned negatively as well (Figure 5B). These values gave a quantitative indication that these two arms tended to simultaneously push in the opposite direction, regardless of the number of arms.

Discussion

Our study newly described the locomotion of brittle stars in a comparative context of four-, five-, six-, and seven-armed intact individuals in a single species. For this purpose, not stereotyping a discrete role of each arm, we introduced a quantitative index which can visualize each arm's degree of being a left or right rower, namely B_α. Coupled with other supportive values, this assessment would bring a unique idea of how 'left and right' emerges in the locomotion of a radially symmetrical animal (Figure 6).

Locomotor modes

In past quantitative studies using five-armed brittle stars, antiphase synchronization of two distant arms has been supported by assessing the stop and start timing of arm movements [11] and by evaluating $E_{\alpha\beta}$ as in our study [12]. This locomotor mode, which is referred to as "breast stroke" or "rowing," is characterized by a leading arm and its side rowing arms [4, 5, 7–12]. Our study figured out that the triplet of left-front-right could appear even in four-, six-, and seven-armed individuals, suggesting that this locomotor mode is determined anteriorly, not laterally or posteriorly. In addition, the two back arms in the five-armed locomotor mode have been often interpreted as passively dragged ones [4, 5, 8, 9, 15]; nevertheless, our study showed that these arms rather worked as weaker rowers since their values of B_{α} ranged either negatively or positively (Figure 2A,C). In six- and seven-armed ophiuroids, back arms following the two strong rowers similarly exhibited a trend of rowers, whereas the backmost ones were usually neutral as to the leftward or rightward bias just like the leading arm (Figures 3A,C, 5A,C). Thus more arms could take charge of 'rowers' especially when a brittle star has more arms.

Although "breast stroke" or "rowing" is a frequently reported locomotor mode in five-armed brittle stars, some studies have also described patterns where there is no leading arm. One is called as "paddling" or "reverse rowing," where a backmost arm is dragged while the other four actively row [5–8, 11]. Such patterns without leading arms have been observed in free movement without experimental stimuli [8, 11] as well as in escape behavior for a short time [16]. In our study using *Ophiactis brachyaspis*, each trial seldom showed such a non-leading pattern (Figures S1–S4). Assuming this brittle star actually switches different locomotor modes, non-leading patterns might be employed only for several seconds after stimuli. In this case, our study might overlook or underestimate this urgent phase since we evenly analyzed one-minute duration after the beginning of the disk's movement. In either case, as far as post-stimulus locomotion was quantified for the fixed period, it seems the locomotor mode with a leading arm is more usual in the intact individuals of the *Ophiactis* species regardless of how many arms they have.

Decision of moving direction

Since brittle stars show no consistent front in behavioral terms as in most echinoderms, every arm can be a leading arm. Astley (2012) described their turning behavior in a short-term series, which was made by changing the roles of arms, not by rotating their body axis. As to an escape situation, several studies have observed that brittle stars avoid open or bright spaces [17, 18], a predator extract [16], and a KCl solution [10]. However, few have probed into how such repellents make a certain reaction per arm to decide the moving direction of a whole individual. Since light and liquid diffuse in water, it is difficult to stimulate only a single target arm. Especially for small brittle stars such as *Ophiactis* species, mechanical stimuli would perform better with the aim to understand how signals from a stimulated arm affect the movements of the other arms.

In our study, two quantitative indices calculated from the filtered angular velocity of arms—B_{α} and $E_{\alpha\beta}$—and one obtained from the original coordinate data—Θ—could together visualize the ophiuroid locomotion without contradiction (Figures 2–5). Postulating each average of the two Θ_{sign}-based patterns as a representative, our numerical results suggest the most frequent locomotion pattern after a mechanical stimulus, in which a leading arm emerges at the *second* neighbor of a stimulated arm while side arms adjacent to the leader synchronously push backward. To realize this bilateral distribution with a high probability, it can be assumed that an afferent signal from an arm makes one of the *first* neighboring arms be an active rower which pushes in the direction of the signaling arm, the *second* neighboring arm be an inactive one which has a less directional preference, and the *third* neighboring arm be another active one which pushes synchronously but oppositely to the *first*'s pushing (Figure 6). Accordingly, the *second* faces forward while the *first*, *third*, and some rear arms work on its both sides. In this model, whether the clockwise or anticlockwise *second* arm becomes a leading arm depends on in which detour the signal dominantly transfers from the stimulated arm, which is determined by some perturbation.

Under our model shown in Figure 6, brittle stars with more arms would have a more risk of 'escape to stimulus.' If the front is placed ideally around the *second* neighboring arm from the stimulus, four-, five-, six-, and seven-armed animals will respectively show 0, 36, 60, and 77 deg in average $|\Theta|$. In fact, the estimation from measured data copied it reasonably—17, 29, 46, and 70 deg, respectively—, and trials where moving direction rather inclined toward the stimulated arm ($90 < |\Theta| \leq 180$) were more frequent as a body had more arms: 0/15, 1/30, 3/30, and 5/15, respectively (Figure 1). Although the 'escape to stimulus' behavior is considered less adaptive, an evolutionary background would explain it. It has been proposed that primitive ophiuroids showed pentaradial symmetry [19, 20], implying that brittle stars had developed a locomotion mechanism which worked optimally for the five-armed body. Some exceptional individuals in arm number, at least the four-, six-, and seven-armed bodies, probably have kept following this initial plan without vital issues. Meanwhile, escaping direction could be more or less bent as a side effect, and the minority of four- and seven-armed ones might be a reflection of some inconvenience in control mechanism or its expression.

Our study has significance to understand how behavioral direction is expressed in a body without antero-posterior and left-right axes. Even when the individual body is round, some direction-making signal could transfer linearly at a local view (Figure 6), just like a wave on a string or neural transmission in the spinal cord. Suppose brittle stars use this strategy, it seems not important how many segments with identical function are counted in the pathway. Otherwise, animal species would never allow individual difference in the number of motile organs.

Inter-arm interaction

Even if arms' function determines as represented in Figure 6, our study remains questions of what kind of interactions mediates such coordination. In neurological aspects, the ophiuroid nervous system principally comprises a circumoral nerve ring in the disk and radial nerve cords extending into each arm [21–25]. Some behavioral studies have supported the essential roles of the circumoral nerve ring in locomotion; menthol-anesthetic experiments indicated its function in initiating locomotion [18]; nerve cut experiments have demonstrated its necessity for coordinating arms [8–10, 26, 27]. For such cases, the inter-arm connection depicted in Figure 6 is recognizable as the circumoral nerve ring. We can assume that the movement of each arm directly reflects neural activity in each radially symmetrical sector, which could be explained even by a couple of neurons. For instance, ophiuroid locomotion would be a useful material for testing "neuron ring" models [28, 29] to know how circularly arranged neurons work in the real world. Taking advantage of the unique individual difference in fissiparous brittle stars, we are able to demonstrate them with different neuron numbers as in computer, which would build a new bridge between theoretical biology and experimental biology.

Besides the crucial role of neural interactions, Kano et al. (2017) found the ophiuroid's ability to immediately change their locomotion patterns after the loss of certain numbers of arms, and then built an ophiuroid-like robot which imitated the adaptive locomotion via a local feedback without any preprogrammed control. Other robotics studies have also suggested the importance of physical interactions in movement coordination which is independent to electrical circuits [30, 31]. Taking account of these researches as well, it is not likely that four- to seven-armed individuals each employ a different central control system while counting the total number of arms. Each arm would just refer to the states of its neighboring arms to realize a coordinated pattern at an individual level, no matter how many arms they own. A trial-by-trial variability in moving direction and other indices (Figures S1–S4) might reflect the influence of physical properties such as arms' posture at each moment, although a circular neural network might dominantly design the average orientation, where the stimulated arm's *second* neighbor faces forward (Figure 6).

Such decentralized autonomous systems must contribute to the ophiuroid evolution that is flexible with the appendage number. It may be a reason why some species such as *Ophiactis brachyaspis* have acquired fissiparity, being capable of drastic morphological changes in a life cycle while retaining its locomotive ability.

Materials and Methods

Animals

We used the fissiparous brittle star *Ophiactis brachyaspis* (Figure S1). In nature, this species densely inhabits the upper and side surfaces of rough rocks or other adherent organisms such as sponges. Some of its arms lie in interstices while some rise from the substrate; suspension feeding ophiuroids show such a posture to capture particles [32]. Animals collected in Shirahama Aquarium, Kyoto University, were reared in a laboratory aquarium (600 × 600 × 600 mm) filled with artificial seawater at 25–28°C with the salinity of 32–35‰ (TetraMarin Salt Pro, Tetra Japan Co, Tokyo, Japan). Body size ranged 1.5–3.0 mm in disk diameter and 5–15 mm in arm length. The number of arms was six in the majority—about 70%—and five for the others. Four- and seven-armed bodies each were found only in one individual.

Behavioral experiments

To investigate locomotion, we chose 10 five-armed individuals and 10 six-armed individuals, in each of which the lengths of arms did not differ by more than twice (c.f. Figure S1). Four- and seven-armed individuals were also targeted; we obtained one for each. Each individual was put in a horizontal flat acrylic case (105 × 75 × 22 mm) filled with 100 mL of artificial seawater from the laboratory aquarium. There were no strong light gradient and no strong wind. Locomotion was recorded in aboral view using a digital camera (EOS8000D, Canon, Tokyo, Japan) with videos saved in MP4 format. We applied mechanical stimuli to arm tips using a toothpick. Stimulating an arm with subsequent observation was defined as one trial. The next trial came at the anticlockwise neighboring arm with an interval of more than two minutes. With repeating this rotation in order, every arm was stimulated at least three times for each individual.

Measurements

Per five- or six-armed individual, we analyzed three trials which showed the longest moving distances of the disk. In the four- and seven-armed cases, we picked out 15 trials with the longest moving distances. Analyzed duration for each trial was one minute after beginning to move the disk following each stimulus (c.f. Videos S1, S2). The stimulated arm in each trial was numbered 1, which was followed anticlockwise by the other arms; α is the index of arms (α = 1, 2, 3, 4, 5 in the five-armed instance). We tracked two coordinate points of the α-th arm using a tracking software Kinovea ver. 0.8.27 (http://www.kinovea.org/, accessed 4 December 2018) at 10 f.p.s.: $P_\alpha(t) = (x_\alpha(t), y_\alpha(t))$—the attachment point between the α-th arm and the disk viewed aborally—and $P'_\alpha(t) = (x'_\alpha(t), y'_\alpha(t))$—the point at half the length of the α-th arm, in terms of the range from the center of disk to the arm tip—at the t-th frame (Figure S2). For the latter, we did not choose each arm's tip because it often rose and showed casual movements seeming irrelevant to locomotion as Matsuzaka et al. (2017) indicated. $P_{\mathrm{cent}}(t)$ was defined as the center of gravity of all arms' $P_\alpha(t)$ (Figure S2). The α-th arm's length (L_α) was defined as the maximum length of the segment $P_\alpha(t)P'_\alpha(t)$ in the analyzed duration. Note that L_α is a variable sampled in each trial, not accounting for the constant length of each arm. Moving distance (S) was measured as the length of $P_{\mathrm{cent}}(1)P_{\mathrm{cent}}(T)$, where T is the total number of frames, i.e. 600 (Figure S2). We assessed moving direction (Θ) as follows:

$$\Theta = \frac{1}{T}\sum_{t=1}^{T}\left(\theta(t)\right) \quad (1),$$

where $\theta(t)$ is the angle made by the two segments $P_c(1)P_c(T)$ and $P_1(t)P_{\mathrm{cent}}(t)$ (Figures S2, S3). Θ, which takes the range from −180 to 180 deg, is 0 deg when the disk moves in the opposite direction of the stimulated arm. A negative or positive value of Θ represents that the disk movement is angled clockwise or anticlockwise, respectively, from the opposite direction of the stimulated arm. For later uses in statistics, the dummy variable Θ_{sign} is defined as

$$\Theta_{\mathrm{sign}} = \begin{cases} 0 & (-180 \le \Theta < 0) \\ 1 & (0 \le \Theta < 180) \end{cases} \quad (2).$$

The segment $P_{\mathrm{cent}}(t)P'_\alpha(t)$ during locomotion swung around $P_{\mathrm{cent}}(t)P_\alpha(t)$, so the α-th arm's angle at the t-th frame ($\varphi_\alpha(t)$) was defined as the angle made by these two segments (Figure S2). $\varphi_\alpha(t)$ is negative or positive when $P_{\mathrm{cent}}(t)P'_\alpha(t)$ is angled clockwise or anticlockwise, respectively, from $P_{\mathrm{cent}}(t)P_\alpha(t)$. $\varphi_\alpha(t)$'s angular velocity ($\omega_\alpha(t)$) was calculated with a five-point moving average method, and then smoothened with a low-pass filter with the cutoff frequency of 1.0 Hz (Figure S3). To quantify to what extent each arm functions as left or right rower, we focused on that returning was faster than pushing in rowing arms. The filtered $\omega_\alpha(t)$ was thus analyzed to evaluate the degree of a leftward or rightward bias in movement, which is represented by B_α (named after "bias"; Figure S3):

$$B_\alpha = \frac{1}{T}\sum_{t=1}^{T}\left(\omega_\alpha(t)^2 \mathrm{sign}\left(\omega_\alpha(t)\right)\right) \quad (3).$$

Assuming that a directional bias results from a speed difference between pushing and returning in each arm, we can rephrase B_α as the α-th arm's degree of being a left or right rower. A largely negative value of B_α represents that the α-th arm moves clockwise faster than anticlockwise, indicating that it slowly pushes leftward and fast returns rightward viewed proximally from the disk. On the contrary, B_α is largely positive when the α-th arm pushes rightward (clockwise). Its value is close to zero when the α-th arm pushes leftward and rightward equally or is dragged without actively returning. We also extracted frequency components in the non-filtered $\omega_\alpha(t)$ of each arm using Fourier transforms. F_α was defined as the frequency at the peak amplitude in the α-th arm.

Besides for B_α, we used the filtered $\omega_\alpha(t)$ to calculate Kano et al.'s (2017) "E_{ij}," namely, the degree of synchronization between two arms:

$$E_{\alpha\beta} = \frac{1}{T}\sum_{t=1}^{T} \omega_\alpha(t)\omega_\beta(t) \quad (4).$$

A negative or positive value of $E_{\alpha\beta}$ represents that the movements of the α- and β-th arms synchronize in the opposite or same direction, respectively. A value around zero represents that the two arms move without strong correlation or are static.

Statistical modeling

We built statistical models for later comparative assessments with the following procedure. Firstly, to examine the structure of a possible bimodality in moving direction, we assume that Θ is subjected to a single von Mises distribution (f_{vM}, 'circular normal distribution'),

$$\Theta[n] \sim f_{\mathrm{vM}}(\mu_\Theta, \kappa_\Theta),\ -\pi \le \mu_\Theta \le \pi,\ \kappa_\Theta \ge 0 \quad (5)$$

or a mixture of two von Mises distributions,

$$\Theta[n] \sim \frac{1}{2} f_{\mathrm{vM}}(-\mu_\Theta, \kappa_\Theta) + \frac{1}{2} f_{\mathrm{vM}}(\mu_\Theta, \kappa_\Theta),\ -\pi \le \mu_\Theta \le \pi,\ \kappa_\Theta \ge 0 \quad (6).$$

Hereafter, n takes one to the total number of trials, so that $\Theta[n]$ denotes the n-th element of Θ. The parameters as random variables μ_Θ—converted to radians for modeling—and κ_Θ are analogous to the mean and the reciprocal of variance, respectively, in normal distribution. For the mixed case, we assume that the two distributions are symmetrical to each other with respect to the position of 0 deg.

Secondly, to understand what brings a trial-by-trial variability of B_α, we parametrize L_α, S, Θ, Θ_{sign}, and F_α each as an explanatory variable for B_α. We assume the normal distribution $f_{\mathrm{norm}}(\mu, \sigma)$, where μ and σ respectively represent the mean and standard deviation (s.d.), as follows:

$$B_\alpha[n, \alpha] \sim f_{\mathrm{norm}}(\mu_{\mathrm{Bi}}[\alpha] + \mu_{\mathrm{Bs}}[\alpha]X, \sigma_{\mathrm{Bi}}[\alpha]),\ \sigma_{\mathrm{Bi}} \ge 0 \quad (7).$$

Here, μ_{Bi}, μ_{Bs}, and σ_{Bi} are arm-by-arm parameters and X is an explanatory variable to which $L_\alpha[n, \alpha]$, $S[n]$, $\Theta[n]$, $\Theta_{\mathrm{sign}}[n]$, or $F_\alpha[n, \alpha]$ is assigned. S, Θ, and Θ_{sign} are common values for all the arms in the same trial. The categorical index Θ_{sign} is to know whether B_α varies continuously by Θ or switches discretely by the sign of Θ. In this instance, μ_{Bs} represents the mean's difference between the negative and positive cases since this variable disappears when Θ_{sign} is zero ($-180 \leq \Theta < 0$) and appears when Θ_{sign} is one ($0 \leq \Theta < 180$). The model without the member $\mu_{\mathrm{Bs}}[\alpha]X$, i.e. without an explanatory variable, is for comparison. In parallel, let us consider whether B_α is better explained by individuality, namely, the quality made by some individual difference other than arm number as to five- and six-armed animals. Consideration of individuality is given to the mean's intercept μ_{Bi}:

$$\mu_{\mathrm{Bi}}[i,\alpha] \sim f_{\mathrm{norm}}(\mu_{\mathrm{B0}}[\alpha], \sigma_{\mathrm{B0}}),\ \sigma_{\mathrm{B0}} \geq 0 \quad (8),$$

$$B_\alpha[n,\alpha] \sim f_{\mathrm{norm}}(\mu_{\mathrm{Bi}}[i,\alpha] + \mu_{\mathrm{Bs}}[\alpha]X, \sigma_{\mathrm{Bi}}[\alpha]),\ \sigma_{\mathrm{Bi}} \geq 0 \quad (9),$$

where i takes one to the total number of individuals (i.e. 10) and the hyperparameters μ_{B0} and σ_{B0} are random variables. Let σ_{B0}, which is common in all arms, have a weakly informative prior as

$$\sigma_{\mathrm{B0}} \sim f_{\mathrm{t}}^{+}(3, 0, 20) \quad (10),$$

where f_t^+ denotes the half t distribution and the parenthetical parameters represent the degree of freedom (v), location (mean when $v > 1$), and scale (s.d. divided by $\sqrt{3}$ when $v = 3$), respectively.

The final modeling is to examine which of Θ and Θ_{sign} is a better explanatory variable for $E_{\alpha\beta}$ in four- to seven-armed animals:

$$E_{\alpha\beta}[n,p] \sim f_{\mathrm{norm}}(\mu_{\mathrm{Ei}}[p] + \mu_{\mathrm{Es}}[p]X, \sigma_{\mathrm{Ei}}[p]),\ \sigma_{\mathrm{Ei}} \geq 0 \quad (11),$$

where μ_{Ei}, μ_{Es}, and σ_{Ei} are pair-by-pair parameters and the explanatory variable X takes $S[n]$, $\Theta[n]$ or $\Theta_{\mathrm{sign}}[n]$. Also considered is the model without the explanatory member $\mu_{\mathrm{Es}}[p]X$.

Employing the Bayesian approach, posterior distribution of each parameter was estimated by the no-U-turn sampler (NUTS) [33]—a variant of Hamiltonian Monte Carlo (HMC) algorithm. In each sampling, we totally obtained 10,000 NUTS samples from four Markov chains, in each of which every 40th generation was sampled in 100,000 iterations after a warmup of 5,000, with the target acceptance rate of 0.8.

Convergence of each parameter was checked by trace plots, the potential scale reduction factor $\hat{R} \leq 1.1$, and the effective sample size $\hat{n}_{eff} \geq 40$, i.e. at least 10 per chain [34]. We assessed the predictability of the models based on WAIC [35, 36], as this criterion is applicable to our models containing mixed distributions (Equation 6) or hierarchical parameters (Equations 8, 9). We developed the resultant statements according to better predicting models, which yielded smaller WAICs than the others considered. For comparison between the models, we referred to the difference as

$$\Delta = 2N(W - W_{\min}) \quad (12).$$

N is the total number of measured samples; multiplication by $2N$ is for the AIC scaling [34]. W is a given model's WAIC while $W_{\min}$ is the smallest WAIC among those of the proposed models, so that Δ is zero in the best performed models. In presenting figures, the posterior predictive distributions of Θ are shown based on the parameters' posterior distributions in a better performed model. To visualize B_α and $E_{\alpha\beta}$ dependent on a better explanatory variable, we obtained the median of each posterior distribution under a model including the explanatory variable not only in the mean but also in the s.d.; Equation 7 or 9 was modified to

$$B_\alpha[n, \alpha] \sim f_{\text{norm}}(\mu_{\text{Bi}}[\alpha] + \mu_{\text{Bs}}[\alpha]X, \exp(\sigma'_{\text{Bi}}[\alpha] + \sigma'_{\text{Bs}}[\alpha]X)) \quad (13),$$

while Equation 11 was replaced by

$$E_{\alpha\beta}[n, p] \sim f_{\text{norm}}(\mu_{\text{Ei}}[p] + \mu_{\text{Es}}[p]X, \exp(\sigma'_{\text{Ei}}[p] + \sigma'_{\text{Es}}[p]X)) \quad (14).$$

Exponentiation in scale is to make the s.d. positive while σ'_{Bi}, σ'_{Bs}, σ'_{Ei}, and σ'_{Es} are random variables without constraints. We did not consider scale's explanatory variables in WAIC comparing terms because the Markov chain simulation failed to converge in many cases. All statistical computation was performed in the software environment R ver. 3.5.1 [37], where Stan codes were compiled and executed by the R package "rstan" [38]. All source codes and data are available from the Figshare repository [39].

Acknowledgments

We thank Mr. Keita Harada in Shirahama Aquarium, Kyoto University, for sending us the fresh individuals of brittle stars from the aquarium. We are grateful to the member of Stan Community (https://mc-stan.org/community/) for suggesting better methods of statistical modeling. This work was partly supported by JSPS KAKENHI (Grant Number 16KT0099) and by JST CREST (Grant Number JPMJCR14D5), Japan.

Competing Interests

The authors declare no competing interests.

References

1. Boffi, E. (1972). Ecological aspects of ophiuroids from the phytal of SW Atlantic Ocean warm waters. Mar. Biol. 15, 316–328.
2. Mladenov, P. V., Emson, R. H., Colpit, L. V., and Wilkie, I. C. (1983). Asexual reproduction in the West Indian brittle star *Ophiocomella ophiactoides* (H.L. Clark) (Echinodermata: Ophiuroidea). J. Exp. Mar. Biol. Ecol. 72, 1–23.
3. Mladenov, P. V., and Emson, R. H. (1984). Divide and broadcast: sexual reproduction in the West Indian brittle star *Ophiocomella ophiactoides* and its relationship to fissiparity. Mar. Biol. 81, 273–282.
4. Romanes, G. J., and Ewart, J. C. (1881). Observations on the locomotor system of Echinodermata. Philos. T. R. Soc. Lond. 172, 829–885.
5. Preyer, W. T. (1887). Die Bewegungen der Seesterne (Berlin: Friedländer).
6. von Uexküll, J. (1905). Studien über den tonus II: die bewegungen der schlangensterne. Z. Biol. 46, 1–37.
7. Glaser, O. C. (1907). Movement and problem solving in *Ophiura brevispina*. J. Exp. Zool. 4, 203–220.
8. Arshavskii, Yu. I., Kashin, S. M., Litvinova, N. M., Orlovskii, G. N., and Fel'dman, A. G. (1976). Types of locomotion in ophiurans. Neurophysiology 8, 398−404.
9. Arshavskii, Yu. I., Kashin, S. M., Litvinova, N. M., Orlovskii, G. N., and Fel'dman, A. G. (1976). Coordination of arm movement during locomotion in ophiurans. Neurophysiology 8, 404−410.

10. Clark, E. G., Kanauchi, D., Kano, T., Aonuma, H., Briggs, D. E., and Ishiguro, A. (2019). The function of the ophiuroid nerve ring: how a decentralized nervous system controls coordinated locomotion. J. Exp. Biol. 222, jeb192104.
11. Astley, H. C. (2012). Getting around when you're round: quantitative analysis of the locomotion of the blunt-spined brittle star, *Ophiocoma echinata*. J. Exp. Biol. 215, 1923–1929.
12. Kano, T., Sato, E., Ono, T., Aonuma, H., Matsuzaka, Y., and Ishiguro, A. (2017). A brittle star-like robot capable of immediately adapting to unexpected physical damage. Roy. Soc. Open. Sci. 4, 171200.
13. Tukey, J. W. (1977). Exploratory Data Analysis (Reading: Addison-Wesley).
14. Gelman, A. (2004). Exploratory data analysis for complex models. J. Comput. Graph. Stat. 13, 755–779.
15. Watanabe, W., Kano, T., Suzuki, S., and Ishiguro, A. (2011). A decentralized control scheme for orchestrating versatile arm movements in ophiuroid omnidirectional locomotion. J. R. Soc. Interface 9, 102–109.
16. Yee, A., Burkhardt, J., and Gilly, W. F. (1987). Mobilization of a coordinated escape response by giant axons in the ophiuroid, *Ophiopteris papillosa*. J. Exp. Biol. 128, 287–305.
17. Cowles, R. P. (1910). Stimuli produced by light and by contact with solid walls as factors in the behavior of ophiuroids. J. Exp. Zool. 9, 387–416.
18. Matsuzaka, Y., Sato, E., Kano, T., Aonuma, H., and Ishiguro, A. (2017). Non-centralized and functionally localized nervous system of ophiuroids: evidence from topical anesthetic experiments. Biol. Open 6, 425–438.
19. Paul, C. R. C., and Smith, A. B. (1984). The early radiation and phylogeny of echinoderms. Biol. Rev. 59, 443–481.
20. Sumrall, C. D., and Wray, G. A. (2007). Ontogeny in the fossil record: diversification of body plans and the evolution of "aberrant" symmetry in Paleozoic echinoderms. Paleobiology 33, 149–163.
21. Cobb, J. L., and Stubbs, T. R. (1981). The giant neurone system in ophiuroids I: the general morphology of the radial nerve cords and circumoral nerve ring. Cell Tissue Res. 219, 197–207.
22. Cobb, J. L., and Stubbs, T. R. (1982). The giant neurone system in ophiuroids III:

the detailed connections of the circumoral nerve ring. Cell Tissue Res. 226, 675–687.

23. Ghyoot, M., Cobb, J. L. S., and Thorndyke, M. C. (1994). Localization of neuropeptides in the nervous system of the brittle star *Ophiura ophiura*. Phylos. T. Roy. Soc. B 346, 433–444.
24. Bremaeker, N. D., Deheyn, D., Thorndyke, M. C., Baguet, F., and Mallefet, J. (1997). Localization of S1- and S2-like immunoreactivity in the nervous system of the brittle star *Amphipholis squamata* (Delle Chiaje 1828). P. Roy. Soc. Lond. B Bio. 264, 667–674.
25. Zueva, O., Khoury, M., Heinzeller, T., Mashanova, D., and Mashanov, V. (2018). The complex simplicity of the brittle star nervous system. Front. Zool. 15, 1.
26. Mangold, E. (1909). Studien zur physiologie des nervensystems der echinodermen. Pflug. Arch. Eur. J. Phy. 126, 371–406.
27. Diebschlag, E. (1938). Ganzheitliches verhalten und lernen bei echinodermen. Z. Vergl. Physiol. 25, 612–654.
28. Suzuki, R., Katsuno, I., and Matano, K. (1971). Dynamics of “neuron ring”. Kybernetik 8, 39–45.
29. Matsuoka, K. (1985). Sustained oscillations generated by mutually inhibiting neurons with adaptation. Biol. Cybern. 52, 367–376.
30. Owaki, D., Kano, T., Nagasawa, K., Tero, A., and Ishiguro, A. (2013). Simple robot suggests physical interlimb communication is essential for quadruped walking. J. R. Soc. Interface 10, 20120669.
31. Owaki, D., and Ishiguro, A. (2017). A quadruped robot exhibiting spontaneous gait transitions from walking to trotting to galloping. Sci. Rep. 7, 277.
32. Warner, G. F. (1971). On the ecology of a dense bed of the brittle-star *Ophiothrix fragilis*. J. Mar. Biol. Assoc. U.K. 51, 267–282.
33. Hoffman, M. D., and Gelman, A. (2014). The No-U-Turn sampler: adaptively setting path lengths in Hamiltonian Monte Carlo. J. Mach. Learn. Res. 15, 1593–1623.
34. Gelman, A., Stern, H. S., Carlin, J. B., Dunson, D. B., Vehtari, A., and Rubin, D. B. (2013). Bayesian Data Analysis, Third Edition (Florida: CPC Press).
35. Watanabe, S. (2009). Algebraic Geometry and Statistical Learning Theory

(Cambridge: Cambridge University Press).

36. Watanabe, S. (2010). Asymptotic equivalence of Bayes cross validation and widely applicable information criterion in singular learning theory. J. Mach. Learn. Res. 11, 3571–3594.
37. R Core Team (2018). R: a language and environment for statistical computing. https://www.R-project.org (accessed 15 November 2018).
38. Stan Development Team (2018). Stan modeling language users guide and reference manual, version 2.18.0. http://mc-stan.org (accessed 15 November 2018).
39. Wakita, D., Kagaya, K., and Aonuma, H. (2019). Data and codes of "Generalized locomotion of brittle stars with an arbitrary number of arms". Figshare. https://doi.org/10.6084/m9.figshare.8019827.v2 (deposited 23 April 2019).

Figures

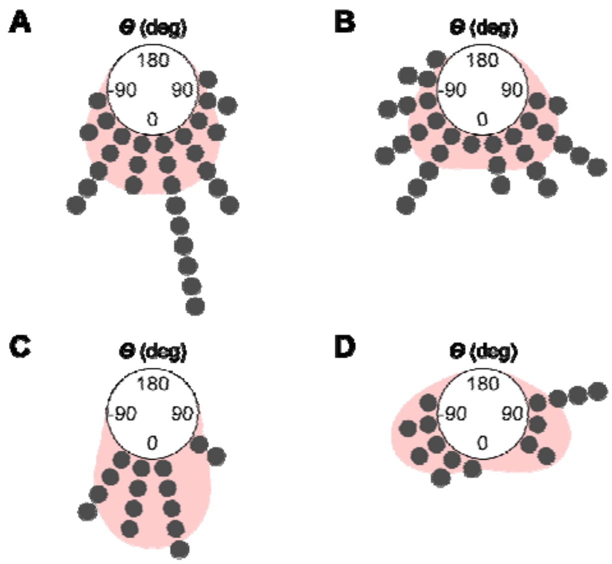

Figure 1. Circular plots of moving direction after mechanical stimuli in the brittle star *Ophiactis brachyaspis*. A: five-armed case (10 individuals, 30 trials). B: six-armed case (10 individuals, 30 trials). C: four-armed case (one individual, 15 trials). D: seven-armed case (one individual, 15 trials). The moving direction Θ is the measured angle based on the position of a mechanically stimulated arm (c.f. Figures S2, S3). Θ is 0 deg when the disk moves in the opposite direction of the stimulated arm, and is negative/positive when the disk movement is angled clockwise/anticlockwise, respectively, from the 0 deg. Each point represents Θ in each trial, which is grouped in a bin divided per 22.5 deg. Density plots on the background represent predictive distributions on the assumption of two symmetrical von Mises distributions.

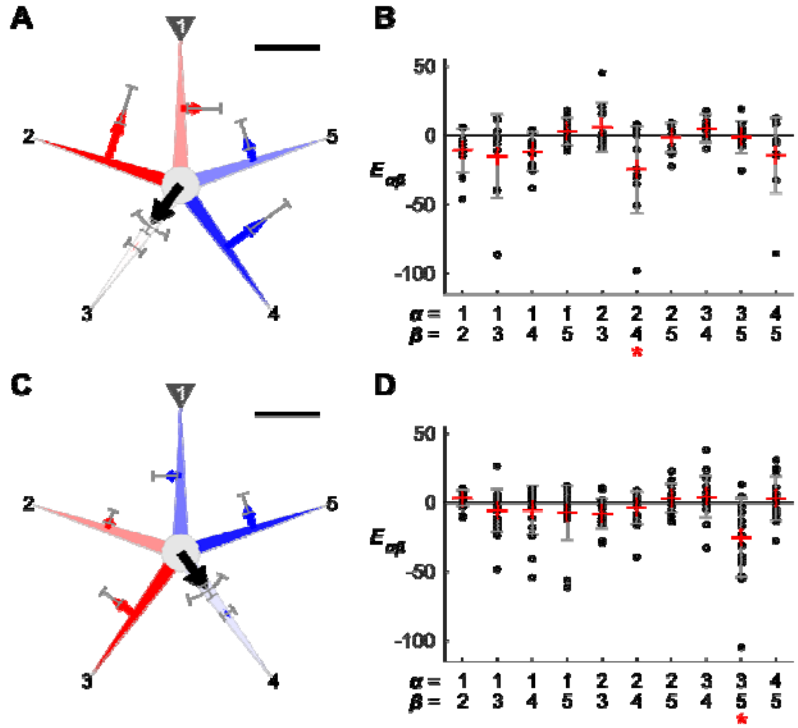

Figure 2. Five-armed locomotion grouped by moving direction in the brittle star *Ophiactis brachyaspis*. A,B: case where moving direction (Θ; c.f. Figures S2, S3) is angled clockwise from the opposite direction of the stimulated arm, i.e. Θ is negative and $\Theta_{sign} = 0$ (eight individuals, 11 trials). C,D: case where Θ is positive (angled clockwise), i.e. $\Theta_{sign} = 1$ (10 individuals, 19 trials); an exemplary locomotion in this case is shown in Video S1. A,C: schematized brittle stars reflecting the resultant quantitative values. Black arrows at the disks represent the measured means of moving distance (S; c.f. Figure S2) by length and the measured means of Θ by angle. Error bars parallel to the disks' arrows show S's standard deviation (s.d.) and arc-shaped error bars represent Θ's s.d. in data. The blue or red arrow at each arm represents the degree of being a left or right rower (B_{α}; c.f. Figures S2, S3), reflecting the absolute median of each posterior mean by arrow length and the median of each posterior s.d. by error bars. When a posterior mean was negative/positive, its blue-leftward/red-rightward arrow extends from its arm, indicating that the arm pushed leftward/rightward (anticlockwise/clockwise), respectively. In each panel, the arm with the maximum absolute value in posterior mean is colored with the most vivid blue/red, while the other arms show lighter blue/red corresponding to the relative values to the maximum. Scale

bars represent 40 mm for S and 50 for B_α. B,D: degree of synchronization between two arms ($E_{\alpha\beta}$ for the α- and β-th arms). Small circles represent measured values. Pair-by-pair red pluses indicate the medians of posterior means while error bars show the medians of posterior s.d. parameters. Negative/positive values represent that the paired movement of the α- and β-th arms synchronized in the opposite/same direction, respectively. Each asterisk indicates the pair with the negatively largest estimated mean, showing remarkable antiphase synchronization. All posterior distributions for both B_α and $E_{\alpha\beta}$ were estimated under a better performed model in terms of WAIC, where Θ_{sign} is an explanatory variable for the mean and s.d.

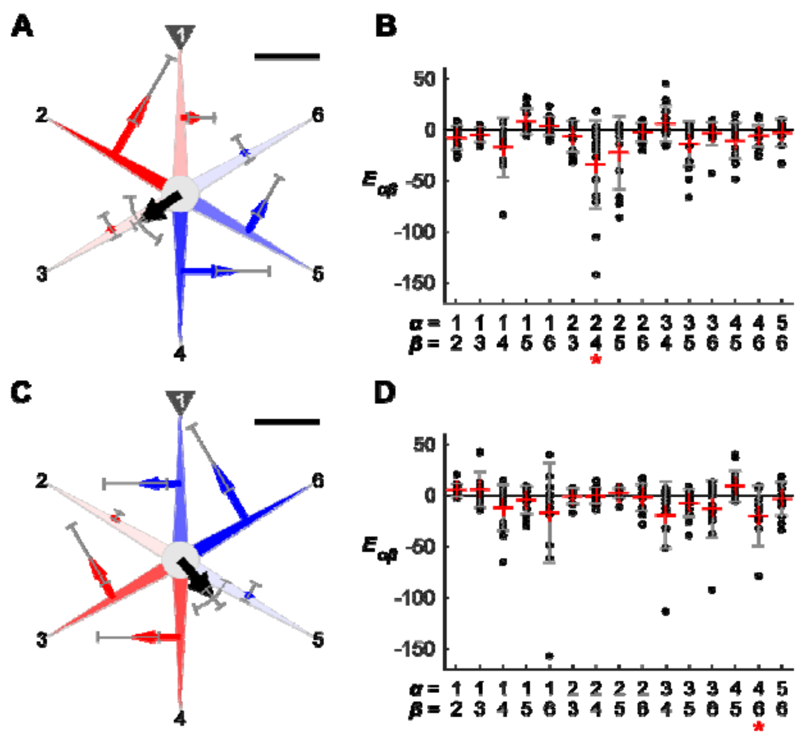

Figure 3. Six-armed locomotion grouped by moving direction in the brittle star *Ophiactis brachyaspis*. A,B: case where $\Theta_{\text{sign}} = 0$ (eight individuals, 16 trials). C,D: case where $\Theta_{\text{sign}} = 1$ (eight individuals, 14 trials); an exemplary locomotion in this case is shown in Video S2. A,C: schematized brittle stars reflecting the resultant quantitative values, as explained in Figure 2. B,D: degree of synchronization between two arms ($E_{\alpha\beta}$ for the α- and β-th arms), as explained in Figure 2.

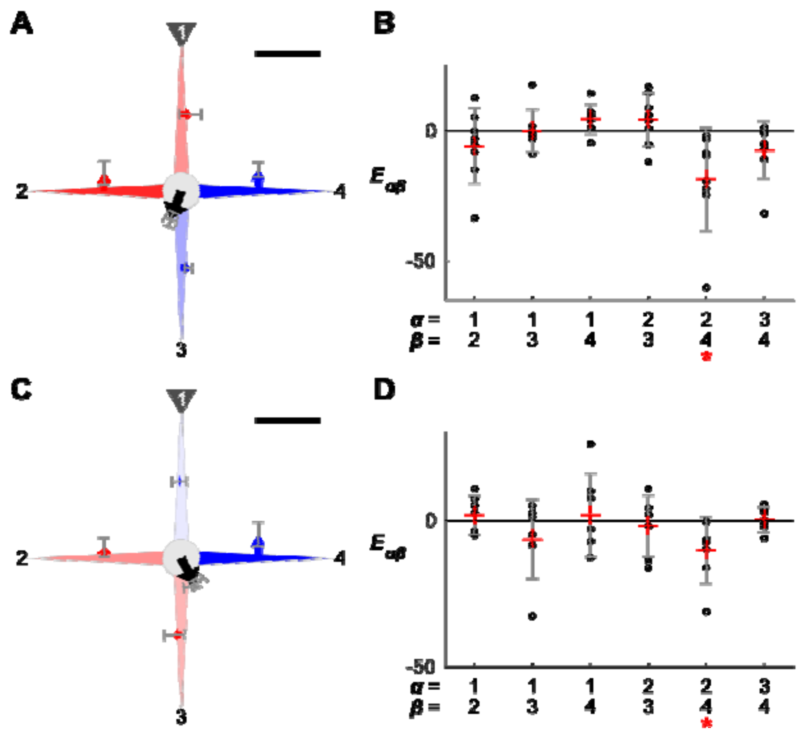

Figure 4. Four-armed locomotion grouped by moving direction in the brittle star *Ophiactis brachyaspis*. A,B: case where $\Theta_{\mathrm{sign}} = 0$ (one individuals, eight trials). C,D: case where $\Theta_{\mathrm{sign}} = 1$ (one individuals, seven trials). A,C: schematized brittle stars reflecting the resultant quantitative values, as explained in Figure 2. B,D: degree of synchronization between two arms ($E_{\alpha\beta}$ for the α- and β-th arms), as explained in Figure 2.

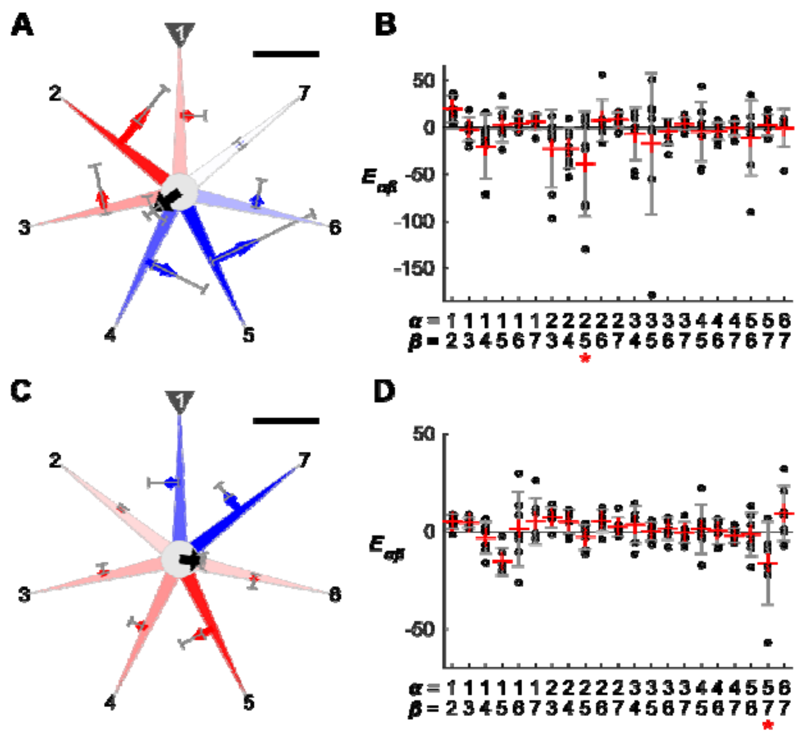

Figure 5. Seven-armed locomotion grouped by moving direction in the brittle star *Ophiactis brachyaspis*. A,B: case where $\Theta_{\mathrm{sign}} = 0$ (one individuals, eight trials). C,D: case where $\Theta_{\mathrm{sign}} = 1$ (one individuals, seven trials). A,C: schematized brittle stars reflecting the resultant quantitative values, as explained in Figure 2. B,D: degree of synchronization between two arms ($E_{\alpha\beta}$ for the α- and β-th arms), as explained in Figure 2.

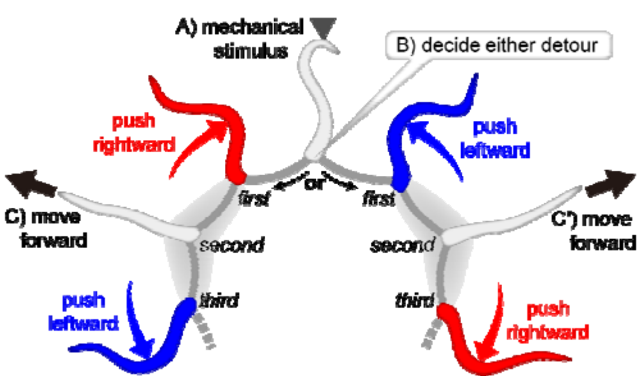

Figure 6. Model of how a mechanical stimulus makes arm-by-arm locomotive movements in brittle stars with an arbitrary number of arms. The stimulated arm makes an afferent signal—(A)—which chiefly transfers in either of the clockwise or

anticlockwise detour through inter-arm connections made by neurons and/or other physical properties. Which detour the signal dominates is determined by some perturbation—(B). Subsequently, one of the *first* neighboring arms to the stimulated arm pushes actively in the stimulus direction, while the *third* neighbor in the same detour pushes oppositely to the *first*. As a result, the *second* arm between the *first* and *third* faces forward in behavioral terms—(C) or (C′).

Tables

Table 1. WAICs of statistical models for Θ, B_α, and $E_{\alpha\beta}$.

Model	Specification		Four-armed			Five-armed			Six-armed			Seven-armed		
			Rank	WAIC	Δ	Rank	WAIC	Δ	Rank	WAIC	Δ	Rank	WAIC	Δ
Θ	**Distribution number**													
1	one		2	0.876	0.917	2	1.192	0.764	2	1.518	5.55	2	1.860	10.7
2	two		1	0.845	**0***	1	1.179	**0***	1	1.425	**0***	1	1.502	**0***
B_α	**Explanatory variable†**	**Individuality†**												
1	no	no	3	4.217	4.94	8	4.671	60.4	5	5.338	58.9	4	4.940	25.7
2	no	yes	—	—	—	9	4.676	61.9	10	5.352	64.0	—	—	—
3	L_α	no	1	4.176	**0***	10	4.679	62.9	9	5.350	63.2	5	4.947	27.1
4	L_α	yes	—	—	—	12	4.688	65.4	12	5.382	74.9	—	—	—
5	S	no	5	4.267	10.9	7	4.670	60.3	7	5.338	59.2	3	4.938	25.2
6	S	yes	—	—	—	11	4.680	63.1	11	5.360	67.0	—	—	—
7	Θ	no	2	4.187	1.29	1	4.469	**0***	2	5.191	6.25	2	4.827	2.03
8	Θ	yes	—	—	—	2	4.477	2.16	4	5.208	12.2	—	—	—
9	Θ_{sign}	no	4	4.230	6.41	3	4.501	9.43	1	5.174	**0***	1	4.818	**0***
10	Θ_{sign}	yes	—	—	—	4	4.505	10.8	3	5.193	6.89	—	—	—
11	F_α	no	6	4.271	11.3	5	4.640	51.0	6	5.338	59.1	6	4.955	28.8
12	F_α	yes	—	—	—	6	4.644	52.3	8	5.347	62.4	—	—	—
$E_{\alpha\beta}$	**Explanatory variable†**													
1	no		1	3.951	**0***	4	4.327	25.6	4	4.440	42.0	3	4.294	9.30
2	S		4	3.974	4.14	3	4.321	22.0	2	4.413	17.5	4	4.320	25.7
3	Θ		2	3.953	0.365	2	4.292	4.90	3	4.416	20.0	2	4.282	1.58
4	Θ_{sign}		3	3.959	1.45	1	4.284	**0***	1	4.394	**0***	1	4.279	**0***

*Δ = 0, bolded, indicating a best supportive model. †Not considered if "no"; otherwise, considered in the mean of normal distribution.

Supplementary Information

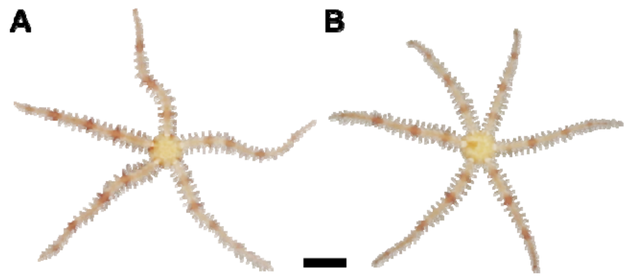

Figure S1. The fissiparous brittle star *Ophiactis brachyaspis*. A: a five-armed individual. B: a six-armed individual. The scale bar represents 2 mm.

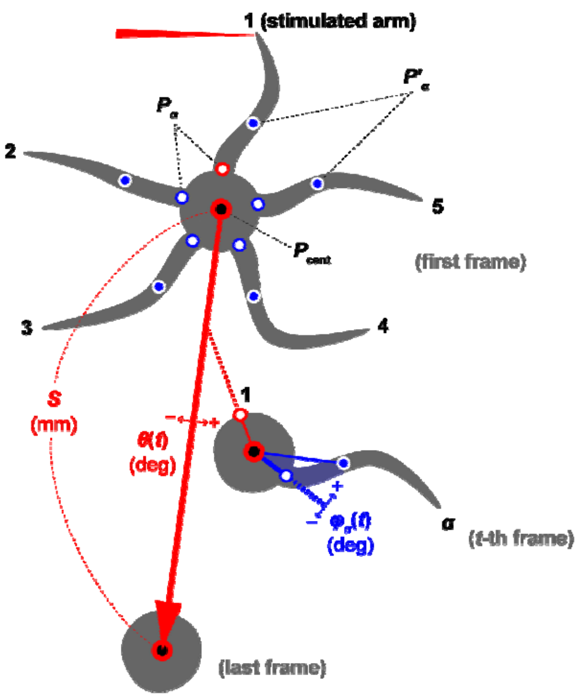

Figure S2. Measurements in the locomotion of the brittle star *Ophiactis brachyaspis*. Schematic five-armed brittle stars are shown at the first (t = 1), t-th, and last (t = 600) frames as an example. Not all arms are shown except for the first frame. The arm index, α, takes 1 to 5, where the stimulated arm is numbered 1. Blue-filled circles indicate the coordinate points of $P'_\alpha(t)$ while open circles show those of $P_\alpha(t)$. Particularly, $P_1(t)$ is indicated by red-lined open circles. The gravity of center of $P_\alpha(t)$, namely $P_{cent}(t)$, is represented by red-lined filled circles. $\varphi_\alpha(t)$ is the arm angle made by $P_\alpha(t)$, $P_{cent}(t)$, and

$P'_\alpha(t)$. $\theta(t)$ is the angle made by the segment $P_{cent}(1)P_{cent}(600)$ and the segment $P_1(t)P_{cent}(t)$, representing the direction of the stimulated arm compared to moving direction. The moving distance S corresponds to the length of the segment $P_{cent}(1)P_{cent}(600)$.

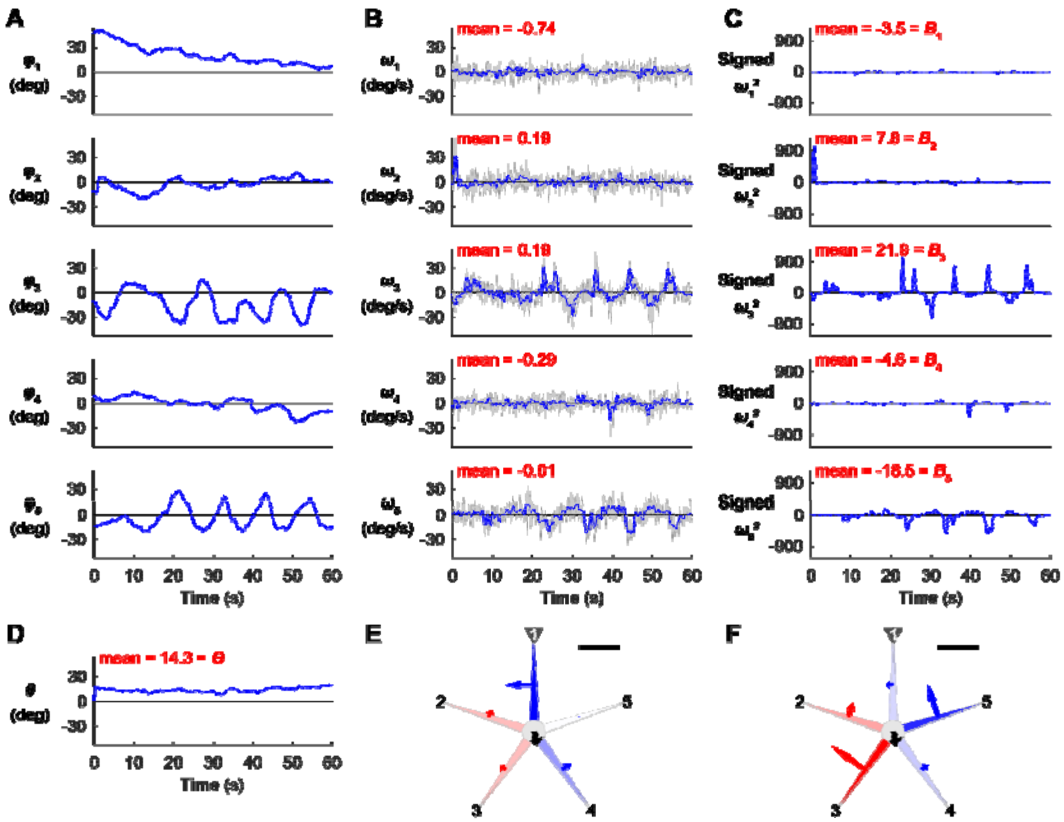

Figure S3. Calculation and visualization in a five-armed example of the locomotion of the brittle star *Ophiactis brachyaspis*. A: temporal change of $\varphi_\alpha(t)$ deg (c.f. Figure S2). B: temporal change of $\omega_\alpha(t)$ deg/s—angular velocity of $\varphi_\alpha(t)$. Background gray plots represent the original data while thicker blue plots show low-pass filtered data. Each plot's "mean" shows the mean value of the filtered $\omega_\alpha(t)$ for $t = 1, ..., 600$. C: temporal change of signed $\omega_\alpha(t)^2$. Each plots' "mean" shows its mean value for $t = 1, ..., 600$, corresponding to B_α—the degree of being a left or right rower in the α-th arm. D: temporal change of $\theta(t)$ deg (c.f. Figure S2). The "mean" shows its mean value for $t = 1, ..., 600$, corresponding to Θ (deg)—moving direction. E: schematized brittle star reflecting the mean $\omega_\alpha(t)$ calculated in B and Θ in D. F: schematized brittle star reflecting B_α in C and Θ in D. In E and F, each gray arrowhead indicates the stimulated arm numbered 1, with the number followed anticlockwise in order. The angles of black arrows at the disks represent Θ. An arm with a negative/positive mean value extends a blue-leftward/red-rightward arrow, respectively, with its length corresponding to the absolute value of its mean. Compared to the mean values of the original $\omega_\alpha(t)$ in E, B_α in F well explains actual locomotion (c.f. Video S1). Note that B_α originally reflects a returning direction by its sign (positive B_α denotes anticlockwise returning), but its schematized arrow here indicates a 'pushing direction' for simply imagining force to the ground (positive B_α denotes clockwise pushing, so apparently opposing the sign in Figure S2). Scale bars represent 1.0 for the mean $\omega_\alpha(t)$ in E and 20 for B_α in F.

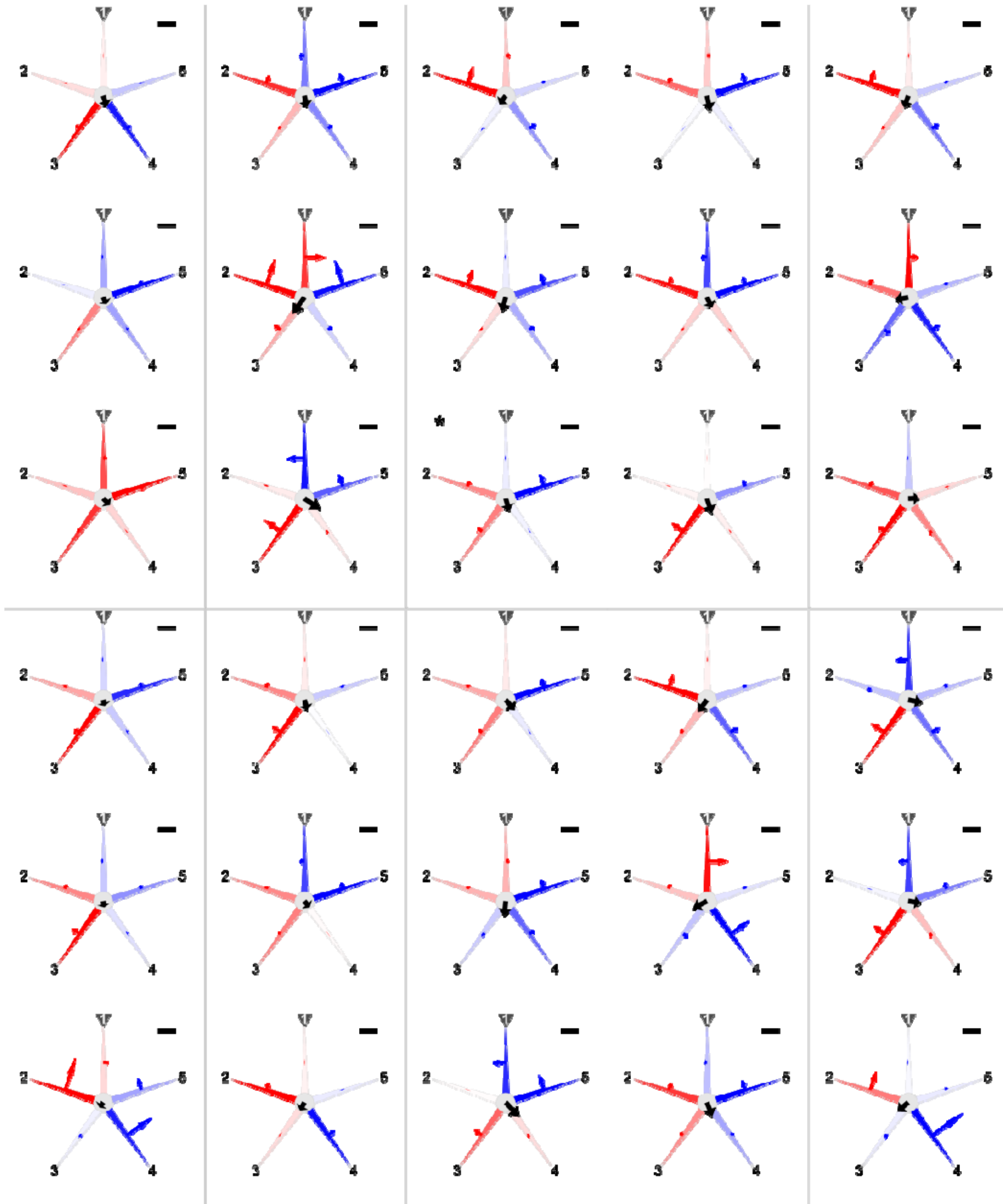

Figure S4. Five-armed trial-by-trial locomotion in the brittle star *Ophiactis brachyaspis*. Three trials were obtained from each of 10 individuals, which are partitioned by gray lines. Black arrows at the disks represent moving distance (*S*; c.f. Figure S2) by length and moving direction (*Θ*; c.f. Figures S2, S3) by angle. An arm with a negative/positive value for the degree of being a left or right rower (B_α; c.f. Figures S2, S3) extends a blue-leftward/red-rightward arrow, respectively, with its length corresponding to $|B_\alpha|$. In each panel, the arm with the maximum $|B_\alpha|$ is colored with the most vivid blue/red, while the other arms show lighter blue/red corresponding to the relative values to the maximum. Scale bars represent 20 mm for *S* and 50 for B_{α}. The asterisked trial (row 3, column 3) is shown in Video S1.

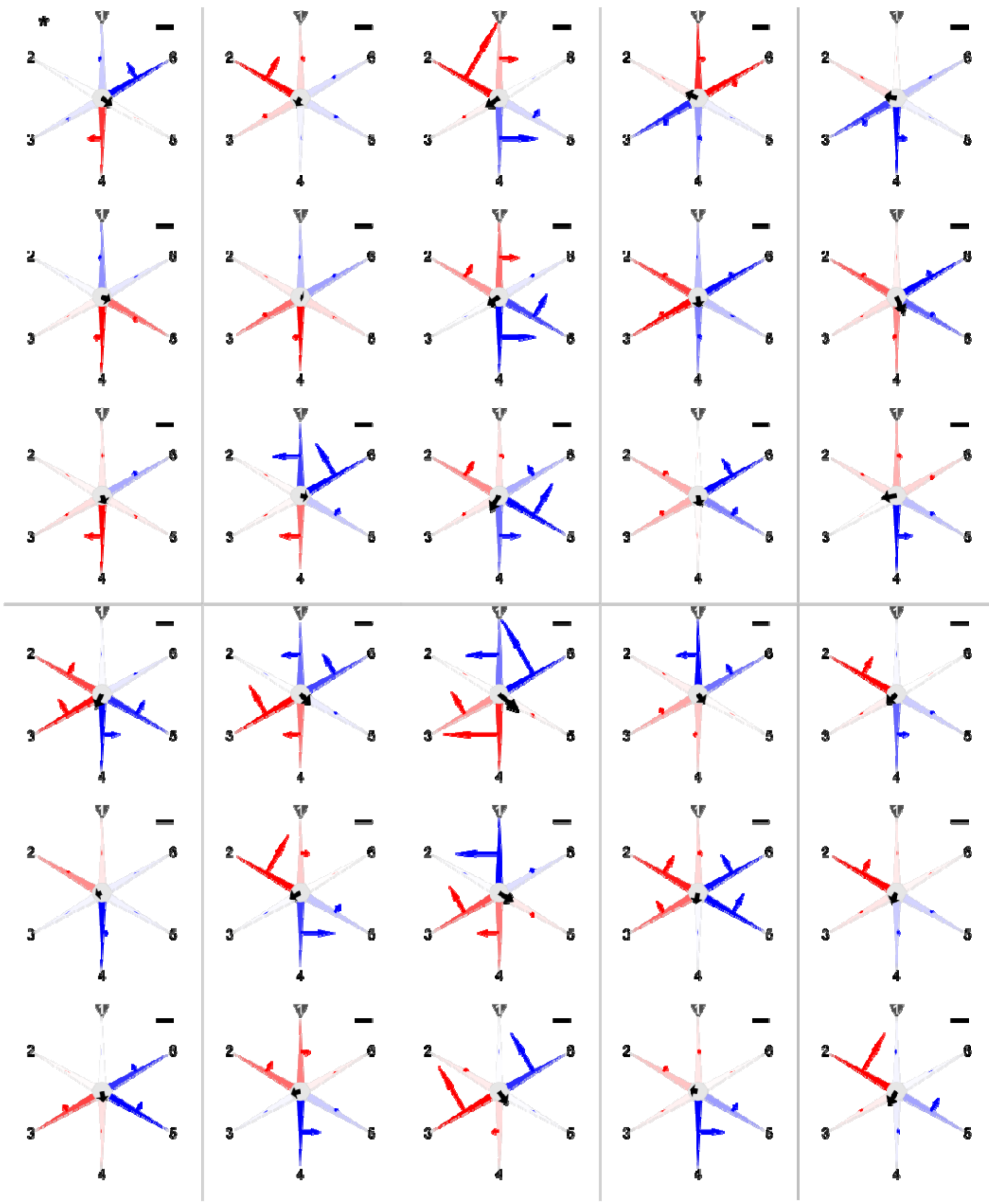

Figure S5. Six-armed trial-by-trial locomotion in the brittle star *Ophiactis brachyaspis*. Three trials were obtained from each of 10 individuals, which are partitioned by gray lines. Results are shown as in Figure S4. The asterisked trial (row 1, column 1) is shown in Video S2.

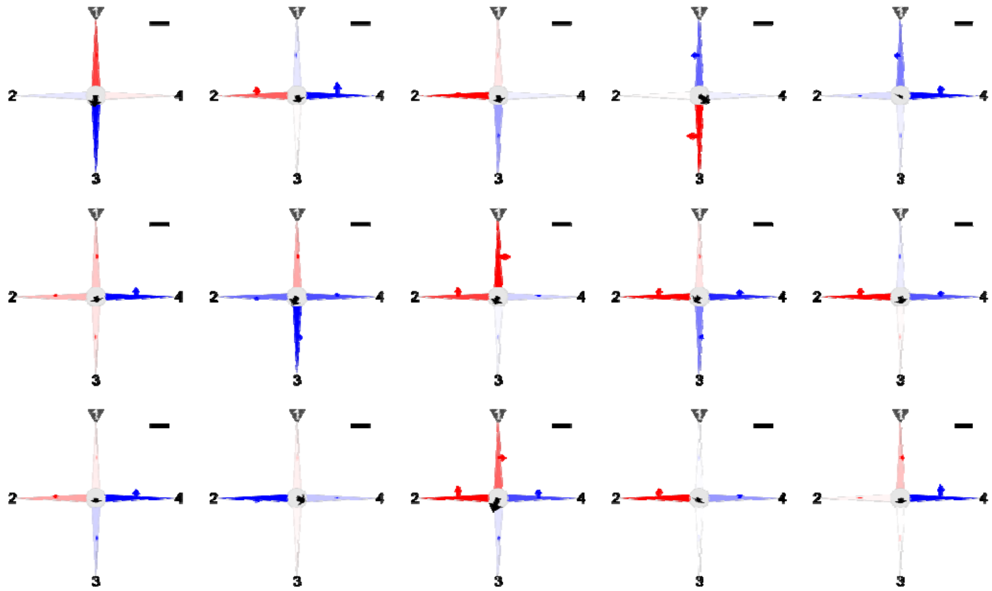

Figure S6. Four-armed trial-by-trial locomotion in the brittle star *Ophiactis brachyaspis*. Fifteen trials were obtained from one individual. Results are shown as in Figure S4.

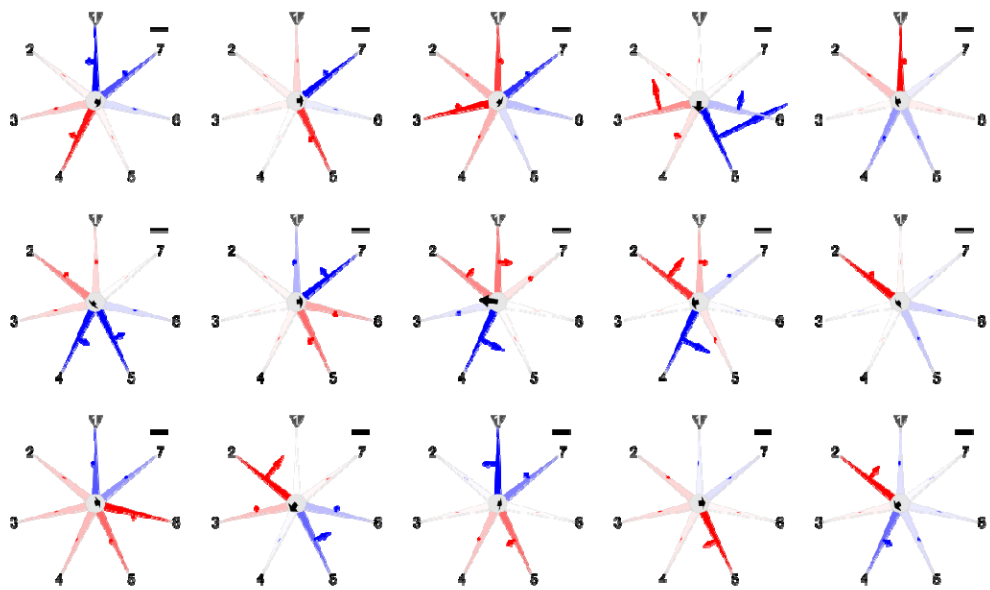

Figure S7. Seven-armed trial-by-trial locomotion in the brittle star *Ophiactis*

brachyaspis**.** Fifteen trials were obtained from one individual. Results are shown as in Figure S4.

Video S1. Locomotion of a five-armed individual of the brittle star *Ophiactis brachyaspis*. Quantitative analysis of this trial is presented in Figure S3. Resultant values are schematized at the asterisked panel in Figure S4.

Video S2. Locomotion of a six-armed individual of the brittle star *Ophiactis brachyaspis*. Resultant values are schematized at the asterisked panel in Figure S5.